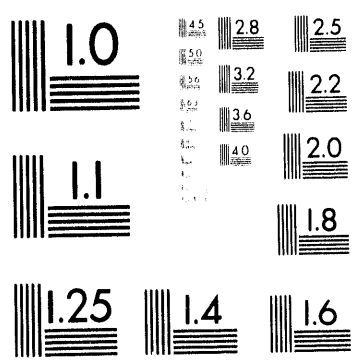
1.0
1.1
1.25
1.4
1.6
1.8
2.0
2.2
2.5
2.8
3.2
3.6
4.0
4.5
5.0
5.6
6.3

1 of 1

Conf-931121--29

LA-UR- 93-3584

Title: **PROCEDURES FOR DETERMINING MATMOD-4V MATERIAL CONSTANTS**

Author(s): **Terry C. Lowe**

Submitted to: **Proceedings of the ASME 1993 Winter Annual Meeting Symposium on "Parameter Estimation for Modern Constitutive Equations", November 28 - December 3, 1993, New Orleans, LA**

Los Alamos
NATIONAL LABORATORY

Form No. 836 R5
ST 2629 10/91

PROCEDURES FOR DETERMINING MATMOD-4V MATERIAL CONSTANTS

Terry C. Lowe
Los Alamos National Laboratory
MST-5, MS G730
Los Alamos, NM 87545

Abstract

The MATMOD-4V constitutive relations were developed from the original MATMOD model to extend the range of nonelastic deformation behaviors represented to include transient phenomena such as strain softening. The improvements that evolved in MATMOD-4V increased the number of independent material constants and the difficulty in determining their values. Though the constitutive relations are conceptually simple, their form and the procedures for obtaining their constants can be complex. This paper reviews in detail the experiments, numerical procedures, and assumptions that have been used to determine a complete set of MATMOD-4V constants for high purity aluminum.

INTRODUCTION

The MATMOD-4V constitutive relations were evolved by Lowe and Miller [1,2] from the MATMOD constitutive relations developed by Miller [3]. MATMOD-4V contains numerous enhancements beyond MATMOD, particularly for representing transient deformation behaviors. The MATMOD-4V equations are derived in [1] and applied for high purity aluminum in [2]. The purpose of this paper is to document the procedures by which the model constants can be derived for a specific material. For simplicity, only the scalar version of MATMOD-4V will be treated. Review of [1] is recommended at this point since space limitations prohibit any explanation of MATMOD-4V and the significance of its four internal state variables R_A, R_B, $F_{def,\rho}$, $F_{def,\lambda}$. Note that the internal state variables will also be referred to as structure variables since they are associated with specific types of microstructural features that evolve during deformation. External variables include the temperature T, the stress σ, and the nonelastic strain rate $\dot{\varepsilon}$. Subscripts are used to indicate special values of any variable.

GENERAL STRATEGY

The application of any constitutive theory requires the determination of model parameters that are specific for the material of interest. The difficulty of obtaining material constants has long been a key factor limiting the widespread application of sophisticated constitutive models such as MATMOD-4V. Values must be determined for the twenty-one constants that exist in the scalar form of the MATMOD-4V equations, given in figure 1. Though the equations appear to be somewhat complex, the procedures for obtaining the constants can be readily understood by first grouping them in the following five categories:

1. Strain rate equation constants,

$$A, B, n, p, (Q^*, T_t);$$

2. Steady state level constants for each structure variable,

$$A_2, A_3, A_4, A_5;$$

3. Structure evolution equation hardening coefficients,

$$H_2, H_3, H_4, H_5;$$

4. Structure variable interaction exponents, and

$$p_2, p_3, p_4, p_5;$$

5. Dynamic/thermal recovery constants for each structure variable.

C_2, C_3, C_4, C_5.

$$\dot{\varepsilon} = B\theta' \left\{ \sinh \left[\frac{\left| \frac{\sigma}{E} - (R_A + R_B) \right|}{\sqrt{F_{def,\rho} + F_{def,\lambda}}} \right]^p \right\}^n \operatorname{sgn}\left[\frac{\sigma}{E} - (R_A + R_B) \right] \qquad \text{(EQ 1)}$$

$$\dot{R}_A = H_2 \left\{ (1 + C_2)\dot{\varepsilon} - \frac{A_2 R_A |\dot{\varepsilon}| \left[\sinh^{-1} \left(\frac{|\dot{\varepsilon}|}{B\theta'} \right)^{\frac{1}{n}} \right]^{p_2 - 1}}{\left[A_4 F_{def,\rho}^{\frac{p}{2(p-1)}} \right]^{p_2}} \right\} - H_2 C_2 B\theta' \left[\sinh (A_2 |R_A|) \right]^n \operatorname{sgn}(R_A) \qquad \text{(EQ 2)}$$

$$\dot{R}_B = H_3 \left\{ (1 + C_3)\dot{\varepsilon} - \frac{A_3 R_B |\dot{\varepsilon}| \left[\sinh^{-1} \left(\frac{|\dot{\varepsilon}|}{B\theta'} \right)^{\frac{1}{n}} \right]^{p_3 - 1}}{\left[A_5 F_{def,\lambda}^{\frac{p}{2(p-1)}} \right]^{p_3}} \right\} - H_3 C_3 B\theta' \left[\sinh (A_3 |R_B|) \right]^n \operatorname{sgn}(R_B) \qquad \text{(EQ 3)}$$

$$\dot{F}_{def,\rho} = H_4 \left\{ (1 + C_4) - \frac{A_4 F_{def,\rho}^{\frac{p}{2(p-1)}} \left[\sinh^{-1} \left(\frac{|\dot{\varepsilon}|}{B\theta'} \right)^{\frac{1}{n}} \right]^{p_4 - 1}}{\left[A_5 F_{def,\lambda}^{\frac{p}{2(p-1)}} \right]^{p_4}} \right\} |\dot{\varepsilon}| - H_4 C_4 B\theta' \left[\sinh \left(A_4 F_{def,\rho}^{\frac{p}{2(p-1)}} \right) \right]^n \qquad \text{(EQ 4)}$$

$$\dot{F}_{def,\lambda} = H_5 \left\{ C_5 + \frac{A_3 |R_B|}{\sinh^{-1} \left(\frac{|\dot{\varepsilon}|}{B\theta'} \right)^{\frac{1}{n}}} - \left[\frac{A_5 F_{def,\lambda}^{\frac{p}{2(p-1)}}}{\sinh^{-1} \left(\frac{|\dot{\varepsilon}|}{B\theta'} \right)^{\frac{1}{n}}} \right]^{p_5} \right\} |\dot{\varepsilon}| - H_5 C_5 B\theta' \left[\sinh \left(A_5 F_{def}^{\frac{p}{2(p-1)}} \right) \right]^n \qquad \text{(EQ 5)}$$

$$\theta' = \begin{cases} exp\left\{ \left[-\frac{Q}{kT_t} \right] \left[ln\left(\frac{T_t}{T} \right) + 1 \right] \right\}, & T \le T_t \\ exp\left(\frac{-Q}{kT} \right), & T > T_t \end{cases} \qquad \text{(EQ 6)}$$

FIGURE 1. Scalar form of MATMOD-4V equations.

The procedures for determining constants within each category are often similar or rely upon a single type of experimental data. Most of the MATMOD-4V constants can be determined directly from mechanical test data. A few constants must be obtained indirectly by relying on assumptions. MATMOD-4V is designed so that its constants remain valid throughout the entire range of temperature and strain rate for which the model is valid. No constant lookup tables [4] or constant adjustment schemes [5] are needed to modify the equations for particular thermal-mechanical deformation conditions.

Procedures for determining each constant value will be briefly outlined following the same sequence that they would be executed to obtain a complete set of values for any metal. The order is important since some procedures rely upon assumed or computed values of other constants. The number of assumptions is minimized by the strategy that is outlined in this paper for obtaining constants for high purity aluminum. In cases where ad hoc assumptions must be used, alternative methods to check assumed constant values are given. Usually, these methods cannot be applied until initial values for all constants have been determined. This restriction affects the degree of effort needed to compute reliable constant values since assumptions made early in the computation strat-

egy may influence subsequent calculations. If there are substantial differences between initially assumed and subsequently determined values, the calculation procedures must be repeated with revised assumptions beginning at the point of the first faulty assumption. Depending upon the quality of assumptions and the desired degree of precision, several iterations may be needed to obtain satisfactory constant values.

The presence of experimental error in mechanical test data makes the determination of material constants imprecise, even for those constants derived directly from simple experiments. In most cases, data analysis serves only to establish upper and lower bounds for a given constant. The choice of a value within these bounds may in some cases involve subjective judgement. Mid-range values are usually chosen initially. Final constant values are obtained by optimization using simple numerical analysis techniques and trial-and-error comparisons of experimental data with model predictions.

STRAIN RATE EQUATION CONSTANTS

Constants for the nonelastic strain rate equation, A,B,n,Q and T_t are determined using steady state creep data obtained in the power law and power breakdown regimes, as outlined below. For steady state deformation, the MATMOD-4V nonelastic strain rate equation reduces to:

$$\dot{\epsilon}_{ss} = B\theta' \left[\sinh \left(A \frac{\sigma_{ss}}{E} \right) \right]^n, \tag{1}$$

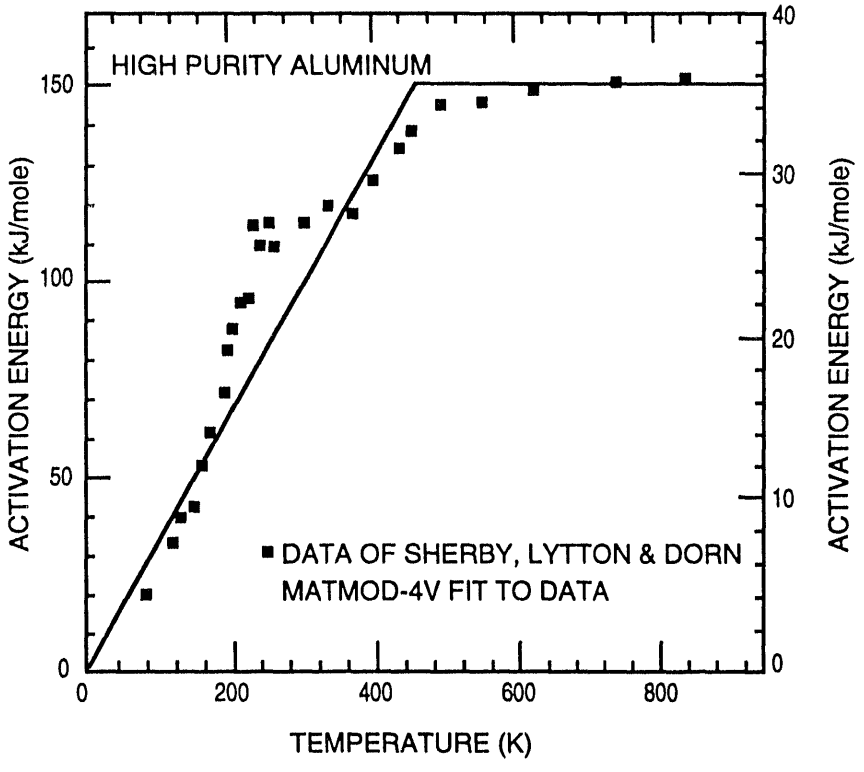

FIGURE 2. Temperature dependence of activation energies for creep of high purity aluminum (data of Sherby, Lytton, and Dorn [6]).

where the effect of temperature upon deformation is represented by a reaction rate relationship θ' as advocated by Dorn and coworkers [7]:

$$\theta' = f\left[exp \left(\frac{-Q}{kT} \right) \right], \tag{2}$$

Q is an activation energy for creep, and k is the gas constant. E in equation 1 is Young's modulus. The subscript ss appearing on variables in equation 1 refers to the specific value of a variable during steady state deformation. Activation energies for creep can be determined using temperature-change tests described in detail by Sherby, Lytton, and Dorn [6]. These investigators found that Q

for aluminum changes with temperature as shown in figure 2. Miller [3] derived a simple mathematical form to approximate this data:

$$\theta' = \begin{cases} exp\{\left[-\frac{Q}{kT_t}\right]\left[ln(\frac{T_t}{T})+1\right]\}, & T \le T_t \\ exp\{-\frac{Q}{kT}\}, & T > T_t \end{cases} \quad (3)$$

where T_t is a transition temperature above which Q is independent of temperature. More recent work by Luthy, Miller, and Sherby [8], showed a different temperature dependence of the activation energy for aluminum at low temperatures. They obtained good agreement between activation energies for self diffusion and those for creep. Sherby, Orr, and Dorn [9] demonstrated the correspondence between activation energies for creep and diffusion for a range of materials. Reasonable descriptions of the temperature dependence of Q can be obtained from diffusion data alone. However, it is preferable to use Q as determined from mechanical testing. For aluminum, θ' is represented by equation 3 where Q and T_t are estimated from the data in figure 2. The only other temperature dependence in MATMOD-4V is that of the elastic modulus E. This data can be easily obtained directly from modulus measurements [10] or from values reported in the literature. The temperature dependence of the modulus of aluminum is represented in MATMOD-4V by fitting a linear equation to the data of Fine [10].

Constants A, B and n may be obtained by a least squares error minimization technique or by the graphical method illustrated in figure 3 where steady creep data [6,12,13,14] is plotted as $\log(\dot{\varepsilon}/\theta')$ versus $\log[\sinh(A\sigma_{ss}/E)]$. The value of A is varied to obtain the best straight line through the data. The slope of the line is n, and its intercept at $\sinh(A\sigma_{ss}/E) = 1.0$ is B.

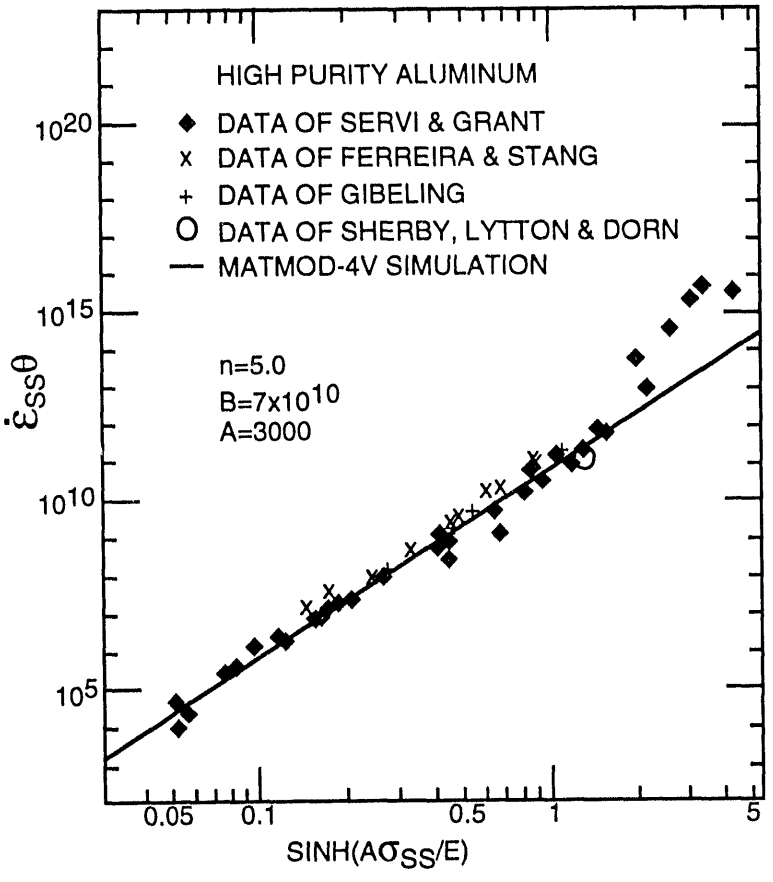

FIGURE 3. Determination of A, B, and n from steady creep data for pure aluminum (data of Sherby, Lytton, and Dorn [6], Ferreira and Stang [12], Servi and Grant [13], and Gibeling [14]).

The same constants B, n, Q and T_t that appear in equation 1 for steady state, also apply to the general form of the MATMOD-4V strain rate equation:

$$\dot{\varepsilon} = B\theta' \left[\sinh \left[\frac{\left| \frac{\sigma}{E} - (R_A + R_B) \right|}{\sqrt{F_{def,\rho} + F_{def,\lambda}}} \right]^p \right]^n \operatorname{sgn}\left[\frac{\sigma}{E} - (R_A + R_B) \right]. \quad (4)$$

One additional constant, p, must be determined for equation 4. Two different methods have been used to compute p. For high purity aluminum one can compute p from room temperature yield strength data for material that has been previously warm worked to steady state at various stresses. When the room temperature yield strength is plotted versus the warm working stress on log-log axes, one observes a power law relationship, as shown in figure 4 [15]. Assuming that the internal stresses introduced by warm working are small, the reciprocal of the power exponent correlating room temperature yield strength with the warm working stress may be taken as p [15].

It is also possible to estimate p from the constant structure creep exponent N. MATMOD-4V predicts that for constant structure (R_A, R_B, $F_{def,\rho}$ and $F_{def,\lambda}$ all constant):

$$N = pn. \quad (5)$$

Unfortunately, reported values of N vary over a wide range, making this method of estimating p unreliable. For aluminum, N values between 6.8 and 10 have been reported [16].

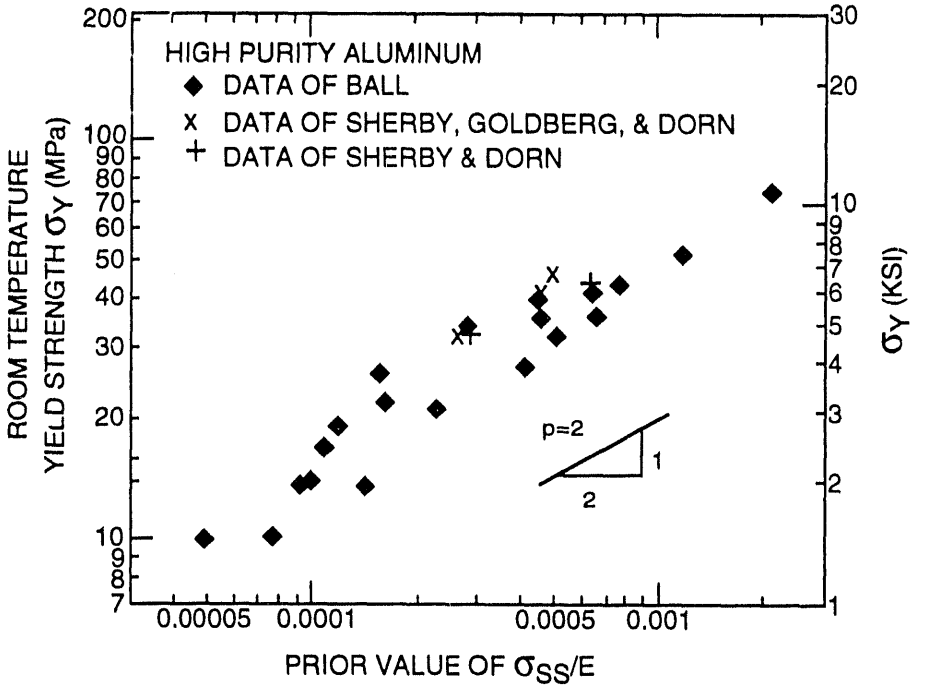

FIGURE 4. Calculation of p from room temperature yield strength data for high purity aluminum warm-worked to various steady state stresses (after Miller and Sherby [15]).

STEADY STATE LEVEL CONSTANTS FOR STRUCTURE VARIABLES A_i

The magnitude of each structure variable during steady state deformation is constant and is determined by the A_i constants through the relations:

$$R_{A,ss} = \frac{C}{A_2} \quad (6)$$

$$R_{B,ss} = \frac{C}{A_3} \quad (7)$$

$$F_{def,\rho,ss}^{\frac{p}{2(p-1)}} = \frac{C}{A_4} \quad (8)$$

$$F_{def,\lambda,ss}^{\frac{p}{2(p-1)}} = \frac{C}{A_5} \tag{9}$$

$$C = \sinh^{-1}\left(\left|\frac{\dot{\varepsilon}_{ss}}{B\theta'}\right|\right)^{\frac{1}{n}}. \tag{10}$$

Experimental measurements of $R_{A,ss}$ and $R_{B,ss}$ [17] may be used to determine A_2 and A_3 directly. However, $F_{def,\rho,ss}$ and $F_{def,\lambda,ss}$ cannot be measured separately by mechanical tests. The relative magnitudes of $F_{def,\rho,ss}$ and $F_{def,\lambda,ss}$ must be assumed initially. Based upon the experimental work of Kassner [18], strengthening from heterogeneous dislocation substructures (attributed to $F_{def,\lambda}$) constitutes a small portion of the isotropic strength, about 10% in 304 stainless steel. Similar experiments have not yet been performed for aluminum, but the same proportionality will be assumed for aluminum:

$$\left(\frac{F_{def,\lambda,ss}}{F_{def,\rho,ss}}\right) = \left(\frac{\frac{C}{A_5}}{\frac{C}{A_4}}\right)^{\frac{2(p-1)}{p}} = \left(\frac{A_4}{A_5}\right)^{\frac{2(p-1)}{p}} = 0.10. \tag{11}$$

The total isotropic hardening,

$$F_{def} = F_{def,\rho} + F_{def,\lambda} \tag{12}$$

can be measured and used to compute A_6 as defined by:

$$F_{def,ss}^{\frac{p}{2(p-1)}} = \frac{C}{A_6} \tag{13}$$

Combining equations 8, 9, 11, 12, and 13, one obtains:

$$A_4 = A_6\left[1 + \left(\frac{A_4}{A_5}\right)^{\frac{2(p-1)}{p}}\right]^{\frac{p}{2(p-1)}}, \tag{14}$$

and,

$$A_5 = A_6\left[1 - \left[1 + \left(\frac{A_4}{A_5}\right)^{\frac{2(p-1)}{p}}\right]^{-1}\right]^{\frac{p}{2(1-p)}} \tag{15}$$

The experimentally determined value of A_6 and an assumed ratio $(A_4/A_5)^{\frac{2(p-1)}{p}}$ may then be used to compute A_4 and A_5. Directional strain softening data [9] may later be used to check the assumed ratio of $F_{def,\lambda}/F_{def,\rho}$. This procedure is described in a latter section since it depends upon the interaction exponents p_i.

HARDENING COEFFICIENTS H_i

Values for the hardening coefficients can be calculated directly from experimental data by using mechanical test techniques that distinguish the structure variables. The relative rates of evolution of each variable are in order of decreasing rate: $\dot{R}_A$, $\dot{F}_{def,\rho}$, $\dot{R}_B$, $\dot{F}_{def,\lambda}$. So in a tensile test, the initial slope of the stress nonelastic strain curve corresponds to changes in R_A while the approach to steady state at large strains is governed by $\dot{F}_{def,\lambda}$. However, distinctions between small strain (microplastic) behavior used to compute H_2 in the $\dot{R}_A$ equation and large strain behavior used to compute H_5 in the $\dot{F}_{def}$ equation may be material dependent. These distinctions follow from the

microstructural significance of each structure variable and must be carefully considered when applied to obtain constants for different metals. The methods used to measure R_A, R_B and F_{def} for the purpose of determining constants for aluminum are discussed in detail in [17].

H_2 can be estimated from the rapid microplastic stress-strain transient during the Bauschinger effect. The slope of the stress-nonelastic strain curve immediately following a strain rate reversal can be related to changes in R_A if it is assumed that the other structure variables are approximately constant. However, this slope changes continuously with R_A since the dynamic recovery rate of R_A depends upon R_A (as seen in the $\dot{R}_A$ equation in figure 1). Thus, it is necessary to measure the slope at the point where R_A, and therefore the dynamic recovery rate of R_A are both equal to zero. The slope of the stress-nonelastic strain curve at this point is proportional to H_2:

$$\left.\frac{d\sigma}{d\varepsilon}\right|_{R_A=0} = E\left.\frac{dR_A}{d\varepsilon}\right|_{R_A=0} = H_2(1+C_2)E. \tag{16}$$

C_2 is unknown, but is typically less than 0.1 and can be neglected. The point where R_A equals zero can be determined from stress-strain hysteresis loops for cyclically saturated deformation. At any strain amplitude, R_A changes through a range approximately equal to twice its saturated peak value $R_{A,SAT}$ within a nonelastic strain ε_{r_2} after each strain rate reversal (shown schematically in figure 5). By symmetry, R_A must equal zero at a stress σ_m midway between the initial reverse yield stress σ_{r_1} and the second reverse yield stress σ_{r_2} at the large offset strain ε_{r_2}. Thus, equation 16 can be used to compute H_2 (neglecting C_2) in terms of easily measured quantities:

$$H_2 = \frac{1}{E}\left.\frac{d\sigma}{d\varepsilon}\right|_{\sigma_m}. \tag{17}$$

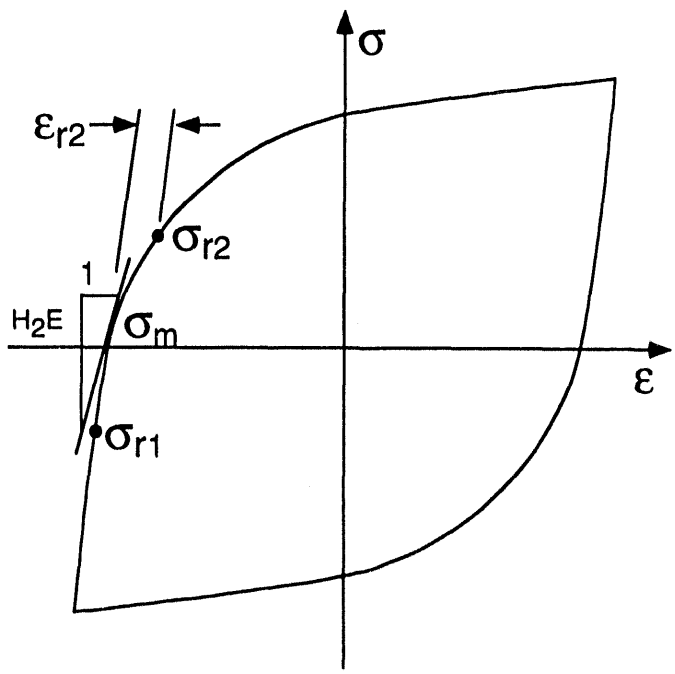

FIGURE 5. Schematic illustrating the calculation of H_2 from cyclic stress-strain data.

H_2 may be computed by graphical analysis as shown in figure 5. Note that H_2 will depend upon the definitions of σ_{r_1} and σ_{r_2}. For aluminum σ_{r_1} and σ_{r_2} have been defined by offset strains of 2×10^{-5} and $2x10^{-3}$, respectively.

H_3 and H_4 are both computed from direct measurements of R_B and F_{def} at small to intermediate strains ($\varepsilon_{r_2} < \varepsilon < 10\varepsilon_{r_2}$) in an initially annealed material. The initial increases in R_B and $F_{def,\rho}$ during monotonic deformation depend exclusively upon the hardening coefficients. R_B and F_{def} may be measured directly during monotonic straining by Bauschinger effect back stress probes [17]. At small to intermediate strains, $F_{def} \approx F_{def,\rho}$ since $F_{def,\rho}$ is generally larger than $F_{def,\lambda}$ and also increases more rapidly. Thus, H_3 and H_4 may be determined from the slope of linear least squares fits to $R_{B-\varepsilon}$ and $F_{def-\varepsilon}$ data, respectively:

$$H_3(1+C_3) = \frac{dR_b}{d\varepsilon}, \tag{18}$$

$$H_4(1+C_4) = \frac{dF_{def}}{d\varepsilon}. \tag{19}$$

Since C_3 and C_4 are small (less than 0.1):

$$H_3 = \frac{dR_B}{d\varepsilon}, \tag{20}$$

$$H_4 = \frac{dF_{def}}{d\varepsilon}. \tag{21}$$

H_5 cannot be computed directly, and depends upon the values of other constants. The rate of increase of $F_{def,\lambda}$ depends upon the product H_5C_5 during initial straining of an annealed material. Since $F_{def,\lambda}$ cannot be readily measured experimentally by mechanical tests, H_5 must be computed indirectly. An upper bound for the product H_5C_5 is provided by the constraint that $F_{def,\lambda}$ initially increase more slowly than $F_{def,\rho}$

$$H_5C_5 < H_4. \tag{22}$$

A temporary value of H_5 is computed using this upper bound after C_5 is determined. After all other constants have been given initial values, H_5 can be estimated from the amount of primary strain to reach steady state during constant stress creep. Since $F_{def,\lambda}$ is the most slowly changing state variable, it will control the amount of strain required to reach steady state. H_5 is adjusted by trial-and-error simulations to match the primary creep strain data. Even though data for only one temperature and stress were used here to obtain H_5, predictions of primary creep by Lowe and Miller [2] show good agreement with data over a wide range of temperature and stress.

INTERACTION EXPONENTS p_i

Low temperature cyclic saturation data is used to determine $p_2, p_3, p_4,$ and p_5. Functional relationships between pairs of structure variables at saturation are fit to experimentally measured values of $R_{A,SAT}$, $R_{B,SAT}$, and $F_{def,SAT}$ where the subscript SAT refers to the peak value of the referenced variable during cyclically saturated deformation.

Small strain amplitude data is used to determine p_5 first. Since C_5 is small, at cyclic saturation $F_{def,\lambda}$ and R_B are related by the expression:

$$\left(\frac{A_5 F_{def,\lambda,SAT}^{\frac{p}{2(p-1)}}}{\sinh^{-1}\left[\left(\frac{|\dot{\varepsilon}|}{B\theta'} \right)^{\frac{1}{n}} \right]} \right)^{p_5} = \frac{A_3 |R_B|_{AVE}}{\sinh^{-1}\left[\left(\frac{|\dot{\varepsilon}|}{B\theta'} \right)^{\frac{1}{n}} \right]} \tag{23}$$

where,

$$|R_B|_{AVE} = -\frac{ln\left[(1+KR_{B,SAT})(1-KR_{B,SAT}) \right]}{K\ ln\left[\frac{(1+KR_{B,SAT})}{(1-KR_{B,SAT})} \right]}$$

and

$$K = \frac{A_3\left[\sinh^{-1}\left(\frac{|\dot{\varepsilon}|}{B\theta'}\right)^{\frac{1}{n}}\right]^{p_3-1}}{\left[A_5 F_{def,\lambda,SAT}^{\frac{p}{2(p-1)}}\right]^{p_3}}.$$

The expression for $|R_B|_{AVE}$, obtained by analytically integrating and then averaging the $\dot{R}_B$ equation over a complete strain cycle, includes the constant p_3, which is still unknown. However, at small cyclic strain amplitudes, $|R_B|_{AVE}$ is nearly unaffected by the value of p_3 and an intermediate value of 0.5 is assigned initially. Experimentally determined values of $F_{def,\lambda,SAT}$ and $R_{B,SAT}$ can be substituted into equation 23 to solve for p_5. Since $F_{def,\lambda,SAT}$ cannot be measured directly, it is necessary to assume that $F_{def,\lambda,SAT}$ and $F_{def,\rho,SAT}$ have nearly the same relative magnitude as $F_{def,\lambda,ss}$ and $F_{def,\rho,ss}$ so that $F_{def,\lambda,SAT}$ may be computed as:

$$F_{def,\lambda,SAT} = F_{def,SAT}\left[1 - \left[1 + \left(\frac{A_4}{A_5}\right)^{\frac{2(p-1)}{p}}\right]^{-1}\right]. \tag{24}$$

After computing p_5, equations 23 and 24 may be employed in computing p_3 using values of $R_{B,SAT}$ and $F_{def,SAT}$ measured at large cyclic strain amplitudes (e.g. +- 0.10). Trial-and-error values of p_3 are used to match the equation to experimental data.

Small strain amplitude cyclic saturation data is used to compute p_2. A relation between $R_{A,SAT}$ and $F_{def,\rho,SAT}$ may be derived by analytically integrating the $\dot{R}_A$ equation:

$$R_{A,SAT} = \frac{F_{def,\rho,SAT}^{\frac{p}{2(p-1)}}(1 + C_2)}{K'}\left[1 - exp\left(\frac{H_2 K' \varepsilon_a}{F_{def,\rho,SAT}^{\frac{p_2 p}{2(p-1)}}}\right)\right] \tag{25}$$

where,

$$K' = \frac{A_2}{A_4^{p_2}}\left[\sinh^{-1}\left(\frac{|\dot{\varepsilon}|}{B\theta'}\right)^{\frac{1}{n}}\right]^{p_2-1}.$$

Given experimentally determined values of ε_a, $F_{def,\rho,SAT}$ and $R_{A,SAT}$, only C_2 and p_2 are unknown in equation 25. However, C_2 is typically very small and can be neglected. Assuming that

$$\frac{F_{def,\rho,SAT}}{F_{def,\lambda,SAT}} \approx \frac{F_{def,\rho,ss}}{F_{def,\lambda,ss}},$$

$F_{def,\rho,SAT}$ may be computed from experimental data as:

$$F_{def,\rho,SAT} = \frac{F_{def,SAT}}{\left[1 + \left(\frac{A_4}{A_5}\right)^{\frac{2(p-1)}{p}}\right]} \tag{26}$$

and substituted into equation 25 with $R_{A,SAT}$ and ε_a to compute p_2.

A relation similar to equations 23 and 25 exists between $F_{def,\rho,SAT}$ and $F_{def,\lambda,SAT}$ from which p_4 can, in principle, be determined. Unfortunately, no means has been developed by which to

experimentally quantify $F_{def,\rho}$ and $F_{def,\lambda}$ simultaneously. However, an indirect method, using directional strain softening data, may be used after all other constants have been given initial values. Since p_4 will have a value between 0 (no interaction between $F_{def,\lambda}$ and $F_{def,\rho}$), and 1 (total coupling of $F_{def,\lambda}$ and $F_{def,\rho}$), an intermediate value of 0.5 can be assumed initially.

RECOVERY RATE CONSTANTS C_i

Data from two types of recovery experiments is needed to compute C_2, C_3, C_4 and C_5. C_2 and C_4 can be computed directly from a back stress recovery experiment [20]. In this experiment, a sample is first cycled to saturation at an elevated temperature to establish a repeatable initial deformation state. Cycling is stopped at zero stress, and the material is allowed to statically recover for a time t. At the end of the recovery period the sample is reloaded in the forward straining direction and a forward yield stress σ_f is measured. The sample is cycled again to saturation, after which another recovery period of equal duration is initiated. At the end of the recovery period the sample is loaded in the reverse direction as though an interrupted Bauschinger test were being performed. A reverse yield stress σ_r is measured. The stresses σ_f and σ_r are used as in a Bauschinger effect test to compute the back stress and the isotropic strength. The back stress recovery test procedure, schematically illustrated in figure 6, is repeated for several recovery periods. Because of the likelihood of errors in back stresses measured in this way, a large strain offset, as used to measure R_B, is used to define σ_r and σ_f. Thus, only recovery of R_B may be estimated by this technique. In fact, it is desirable that R_A completely recover during the recovery period, so that any remaining directional effect may be associated with R_B. For this reason, data for longer recovery times is preferred for determining the recovery kinetics of R_B. Minimal values of R_A at longer times also ensure that recovery is nearly static.

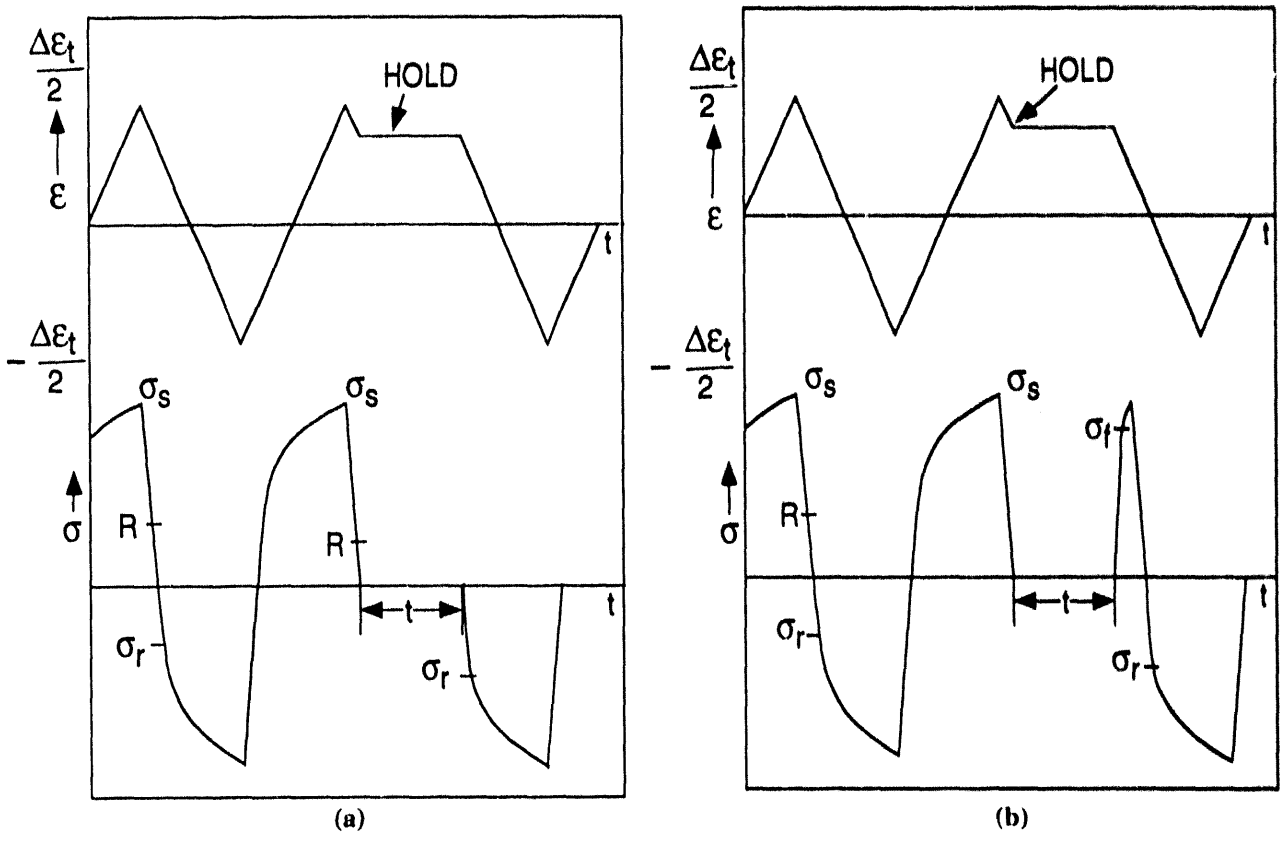

FIGURE 6. Schematic illustration of the method for estimating the recovery of the long range internal stress variable R_B during zero-stress annealing periods. The reverse yield stress σ_r after a period of recovery is measured as shown in (a) and the forward flow stress σ_f is shown in (b).

C_3 may now be determined by numerical analysis. First, a least squares polynomial (or other suitable function) is fit to the $R_B - t$ recovery data to define $\dot{R}_B = f_1(R_B)$. This function may then

be compared with the MATMOD-4V R_B recovery function which also expresses $\dot{R}_B$ as a function of R_B:

$$\dot{R}_{B,\,recovery} = -C_3 H_3 B \left[\theta' \sinh\left(A_3 R_B\right)\right]^n. \tag{27}$$

C_3 is the only unknown constant in equation 27 and may be calculated for a given value of R_B as:

$$C_3 = \frac{f_1(R_B)}{H_3 B \left[\theta' \sinh\left(A_3 R_B\right)\right]^n}. \tag{28}$$

The same procedure is used to compute C_4. Since $F_{def,\rho} \approx F_{def}$ experimental measurements of recovery of isotropic strength are interpreted in terms of recovery of $F_{def,\rho}$. A function is fit to the data to describe the rate of recovery of $\dot{F}_{def,\rho}$.

$$\dot{F}_{def,\rho} = f_2\left(F_{def,\rho}\right).$$

This function is compared with the MATMOD-4V expression for static recovery of $F_{def,\rho}$ and C_4 is computed as:

$$C_4 = \frac{f_2\left(F_{def,\rho}\right)}{H_4 B\left[\theta' \sinh\left(A_4 F_{def,\rho}^{\frac{p}{2(p-1)}}\right)\right]^n}, \tag{29}$$

for any $F_{def,\rho}$. The effects of scatter in the experimental data or possible disagreement between $f_2\left(F_{def,\rho}\right)$ and the MATMOD-4V recovery function may be minimized by computing C_4 for several values of $F_{def,\rho}$ and calculating an average.

The remaining recovery constants, C_2 and C_5 are determined by comparing data from stress drop experiments with MATMOD-4V simulations. A stress drop experiment involves creeping a sample at constant temperature and constant stress and then instantaneously reducing the stress to some fraction of the initial stress [21, 22]. There is an immediate decrease in the creep rate which depends upon the magnitude of the stress drop. For large stress drops the creep rate may become negative before forward straining at the reduced stress is resumed. The creep rate transients that occur between the instant of the stress drop and the time that a steady state creep condition is reached at the reduced stress are determined by the changes in the structure variables. The relative contributions of strain-activated and thermal recovery greatly influence the time before forward creep is resumed after a large stress drop and the time to reach a new steady state at the reduced stress. These two times are indicated as t_1 and t_2, respectively, in figure 7.

In MATMOD-4V simulations of stress drops, the time to resumption of forward creep, t_1, is almost exclusively dependent upon C_2. Simulations using an assumed value of C_5 and various values of C_2 can be compared with experimental data to select an appropriate C_2 value. In practice, it is difficult to measure a forward strain rate less than 10^{-8}sec^{-1}, so that t_1 must be redefined as the time to reach an experimentally measurable strain rate. Times to resume forward creep in stress drop experiments using aluminum have been reported by Gibeling [14].

The time t_2 to reach a new steady-state creep rate at a reduced stress is influenced by C_2, C_3, C_4, and C_5. But at this point C_5 is the only variable which remains undefined. Thus C_5 can be selected to match experimental measurements of t_2 with MATMOD-4V simulations of the same experiments. Though all four C_i constants influence t_2, it is most appropriate to use C_5 to fit the MATMOD-4V predictions to the data since $F_{def,\lambda}$ is the most slowly changing structure variable. Furthermore, Ferreira and Stang [12] have found a direct correlation between changes in subgrain size (corresponding to $F_{def,\lambda}$) and the approach to steady state following a stress drop.

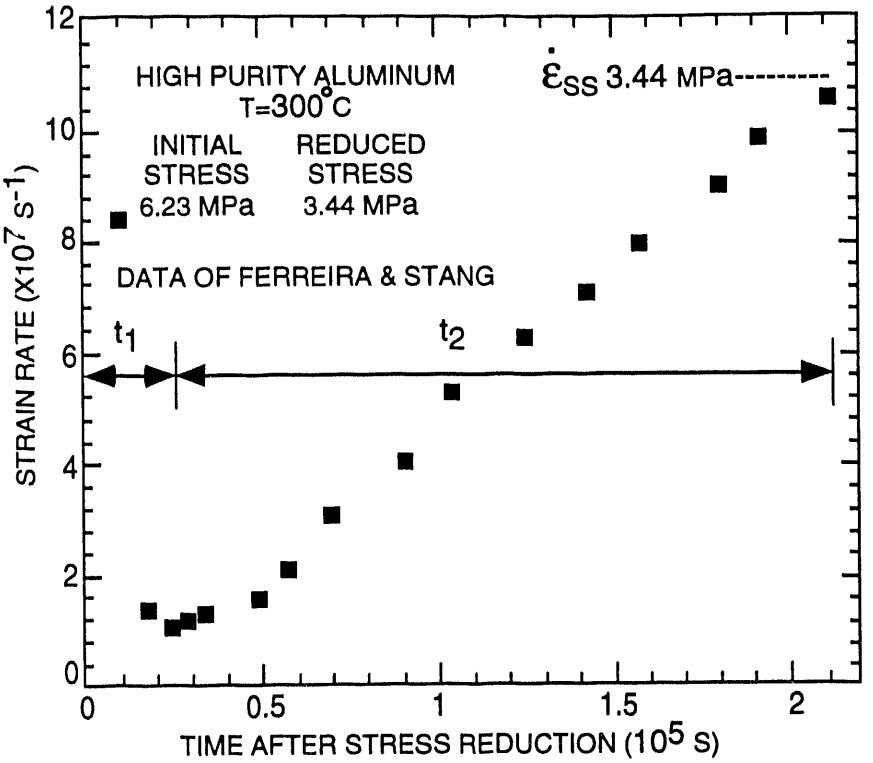

FIGURE 7. Transients in the strain rate following a large stress reduction during creep. The times required to resume forward creep (t_2) and to reach steady state at the new stress (t_2) are indicated (data of Ferreira and Stang [12]).

ITERATION TO OBTAIN FINAL CONSTANT VALUES

After initial values have been assigned to all constants, simulations of a wide range of experimental behaviors may be performed to test the choice of constant values and guide refinements to obtain final values. The initially assumed values of A_4, A_5 and p_4 can be refined using strain softening data. Directional strain softening data [19] offers a unique means of determining the relative strength contributions of $F_{def,\rho}$ and $F_{def,\lambda}$.

In simulations of directional strain softening, $F_{def,\rho}$ and $F_{def,\lambda}$ exhibit different sorts of behavior when uncoupled; $F_{def,\rho}$ always increases toward a saturated value while $F_{def,\lambda}$ may decrease following a strain rate reversal due to an interaction with R_B as seen in figure 8. This decrease is the essence of directional strain softening. Thus, decreases in isotropic strength during directional strain softening may be directly attributed to the reduction of $F_{def,\lambda}$ in the absence of any coupling with $F_{def,\rho}$. One could estimate the relative magnitudes of $F_{def,\rho}$ and $F_{def,\lambda}$ from the magnitude of directional strain softening, thereby allowing a direct means to compute A_4 and A_5. However, if $F_{def,\rho}$ is closely coupled to $F_{def,\lambda}$ (large p_4) then both $F_{def,\rho}$ and $F_{def,\lambda}$ will decrease during directional strain softening. Additional information is then needed to simultaneously distinguish $F_{def,\rho}$ from $F_{def,\lambda}$ and thereby determine A_4, A_5 and p_4.

The strain amplitude dependence of directional softening during cyclic deformation allows the reduction in isotropic strength to be attributed to either a close coupling of $F_{def,\rho}$ with $F_{def,\rho}$ or a large relative magnitude of $F_{def,\rho}$. If $F_{def,\rho}$ and $F_{def,\rho}$ are totally coupled ($p_4 = 1$), then directional softening, observed as inversion in hysteresis loop curvature, would be predicted at almost all strain amplitudes. If instead $F_{def,\lambda}$ and $F_{def,\rho}$ are decoupled ($p_4 = 0$) then directional softening would be possible only at larger strain amplitudes where the decreases in $F_{def,\lambda}$ during cyclic deformation are large.

Thus A_4, A_5 and p_4 may be uniquely defined by concurrently using experimental data on: 1) the magnitude of the $F_{def,ss}$, 2) the loss of isotropic strength during directional strain softening, and 3) the strain amplitude dependence of directional strain softening during cyclic deformation. These constants are adjusted by trail-and-error until simulations of directional strain softening correspond to the experimental data.

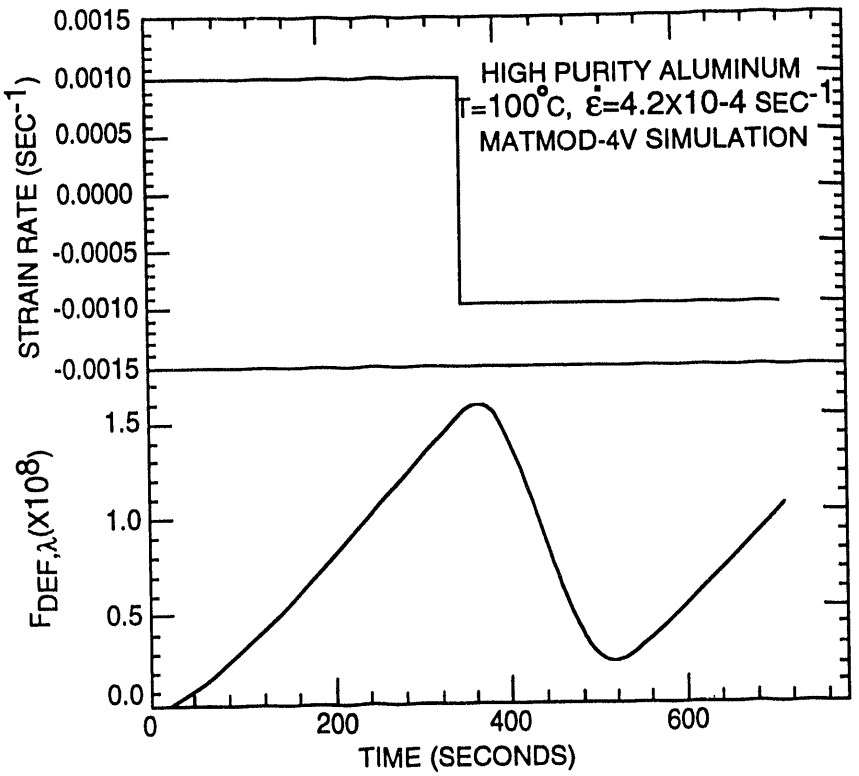

FIGURE 8. MATMOD-4V simulation of a strain direction reversal showing the reduction of $F_{def,\lambda}$ which results from the interaction between R_B and $F_{def,\lambda}$ in the $\dot{F}_{def,\lambda}$ equation.

If substantial changes in A_4 and A_5 are indicated by the iteration to define A_4/A_5 and p_4, then p_2, p_3, p_5, C_2, C_4 and C_5 must all be recomputed using the new A_4/A_5 ratio. Then the iteration to check p_4 and A_4/A_5 must also be repeated. If further changes in A_4 and A_5 are warranted, then this cycle is continued until satisfactory values of all constants are found. For high purity aluminum, only one iteration cycle was required to obtain satisfactory constant values.

SUMMARY OF EXPERIMENTAL REQUIREMENTS TO OBTAIN CONSTANTS

All MATMOD-4V constants can be derived from mechanical test data. However, the number of different tests and precision of measurement required makes the constant derivation process lengthy. The apparatus and tests for determining a complete set of MATMOD-4V constants are summarized in Table 1. Two types of test apparatus are needed, a constant stress creep machine with provisions for rapid load and temperature changes and a low-backlash reverse torsion machine with microprocessor control. Both machines should be equipped with high strain resolution measurement devices. Digital data acquisition is desirable, particularly if strain measurement is limited by system resolution or electrical noise.

Most of the test techniques used in determining constants are fairly standard and easily executed. Only the back stress recovery experiment and the high strain resolution Bauschinger effect measurements are unusual. Bauschinger effect back stress measurements and data analysis are discussed in [20]. The final constant values determined for pure aluminum are listed in Table 2.

Experiment			Constants
Apparatus	Test	Measure	
Creep machine	Constant stress creep at various temperatures and stresses	-Primary creep strain $-\dot{\varepsilon}_{ss}$	H_5 B,n
	Temperature change during creep	$\dot{\varepsilon}$	Q, T_4
	Stress drop during creep	$\dot{\varepsilon}$	C_2, C_5
Reverse torsion machine	Constant strain rate test to steady state with periodic Bauschinger effect back stress probes	$-R_A$, R_B, F_{def} as a function of ε $-R_{A,ss}$, $R_{B,ss}$, $F_{def,ss}$	H_3, H_4 A_2, A_3, A_6
	Low temperature cyclic saturation at: small strain ampitude large strain amplitude	σ R_A, R_B, F_{def} R_A, R_B, F_{def}	H_2 p_2, p_5 p_3
	Back stress recovery experiment	R_B, F_{def}	C_3, C_4
	Large strain amplitude cyclic deformation with mid-cycle Bauschinger effect back stress probes	R_A, R_B, F_{def}	p_4, A_4, A_5

TABLE 1. Summary of Equipment and Experiments Needed to Determine MATMOD-4V Constants

Constant	Value	Constant	Value
Q*	33,500 cal/mole	H_4	1.0×10^{-7}
T_t	461K	H_5	1.0×10^{-6}
B	7×10^{10} sec^{-1}	C_2	2.0×10^{-3}
n	5.0	C_3	2.0×10^{-3}
p	2.0	C_4	2.0×10^{-8}
A_2	7630	C_5	2.0×10^{-8}
A_3	2.0×10^{5}	p_2	0.25
A_4	1.154×10^{8}	p_3	0.10
A_5	1.000×10^{8}	p_4	0.10
H_2	0.3	p_5	0.50
H_3	1.5×10^{-4}		

TABLE 2. MATMOD-4V Constants for High Purity Aluminum

SUMMARY

The procedures for obtaining equation constants for MATMOD-4V have been outlined and applied to obtain constants for high purity aluminum. Predictions of deformation response and comparisons with experimental data using these constants have been shown by Lowe and Miller [2]. The amount of time and effort required to obtain constants will vary, depending primarily upon the availability of the experimental data summarized in Table 2. Assuming all required data is available, a complete set of constants can be determined by a skilled numerical analyst in approximately one month, or less. The most difficult part of obtaining a reliable set of constants is performing trial simulations to evaluate the impact of assumptions made early in the derivation process and to assess parameter sensitivity.

ACKNOWLEDGEMENTS

The author would like to express special thanks to Jennifer McDonald who patiently and skillfully formatted and illustrated this paper. This work was performed under the auspices of the U.S. Deopartment of Energy.

REFERENCES

1. T.C. Lowe and A.K. Miller, 1984, "Improved Constitutive Equations for Modeling Strain Softening-- Part I: Conceptual Development," *Journal of Engineering Materials and Technology*, Vol. 106, pp. 337-342.
2. T.C. Lowe and A.K. Miller, 1984, "Improved Constitutive Equations for Modeling Strain Softening-- Part II: Predictions for Aluminum," *Journal of Engineering Materials and Technology*, Vol. 106, pp. 343-348.
3. A.K. Miller, 1975, "A Unified Phenomerological Model for the Monotonic, Cyclic, and Creep Deformation of Strongly Work-Hardening Materials," Ph.D. dissertation, Stanford University.
4. R.D. Krieg, J.C. Swearengen, and R.W. Rohde, 1978, "A Physically-Based Internal Variable Model for Rate-Dependent Plasticity," *Inelastic Behavior of Pressure Vessel and Piping Components*, PVP-PB-028, ASME, p. 15.
5. R.W. Rohde, W.B. Jones, and J.C. Swerengen, 1981, "Deformation Modeling of Aluminum: Stress Relaxation, Transient Behavior, and Search for Microstructural Correlations," *Acta Met.*, Vol. 29, pp 41-52.
6. O.D. Sherby, J.L. Lytton, and J.E. Dorn, 1957, "Activation Energies for Creep of High Purity Aluminum," *Acta Met.*, Vol. 5, pp. 219-227.
7. J.E. Dorn, 1957, "The Spectrum of Activation Energies for Creep," *Creep and Recovery*, ASM, Cleveland, pp. 255-283.
8. H. Luthy, A.K. Miller, and O.D. Sherby, 1980, "The Stress and Temperature Dependence of Steady-State Flow at Intermediate Temperatures for Pure Polycrystalline Aluminum," *Acta Met.*, Vol. 28, pp. 169-178.
9. O.D. Sherby, R.L. Orr, and J.E. Dorn, 1954, "Creep Correlations of Metals at Elevated Temperatures," *Trans. AIME*, Vol. 200, 71-80.
10. M.E. Fine, 1957, "Apparatus for Precise Determination of Dynamic Young's Modulus and Internal Friction at Elevated Temperatures," *Rev. of Sci. Instr.*, Vol. 28, 643- 645.
11. T. Tanaka, 1981, unpublished work, Stanford University.
12. I. Ferriera and R.G. Stang, 1979, "The Effect of Stress Reductions on the Creep Behavior and Subgrain Size in Aluminum Deformed at 573 K," *Matls. Sci. and Engg.*, Vol. 38, pp. 169-174.

13. I.S. Servi and N.J. Crant, 1951, "Creep and Stress Rupture Behavior of Aluminum as a Function of Purity," *J. Metals*, Vol. 141, pp. 909-916.

14. J.C. Gibeling, 1979, "The Use of Stress Change Experiments to Study the Mechanisms of Elevated Temperature Deformation," Ph.D. dissertation, Stanford University.

15. A.K. Miller and O.D. Sherby, 1978, "A Simplified Phenomenological Model for Nonelastic Deformation: Predictions of Pure Aluminum Behavior and Incorporation of Solute Strengthening Effects," *Acta Met.*, Vol. 26, pp. 289-304.

16. J.C. Gibeling and W.D. Nix, 1982, "Anomalous and Constant Structure Creep Transients in Pure Aluminum," *Proceedings of the 6th International Conference on the Strength of Metals and Alloys*, Melbourne, Australia, Aug. 16-20, pp. 613- 618.

17. T.C. Lowe, 1983, "New Concepts in Modeling Strain Softening," Ph.D. dissertation, Stanford University.

18. M.E. Kassner, 1981, "The Separate Roles of Forest Dislocations and Subgrains in the Isotropic Hardening of Type 304 Stainless Steel," Ph.D. dissertation, Stanford University.

19. T.C. Lowe and A.K. Miller, 1983, "The Nature of Directional Strain Softening," *Scripta Metallurgica*, Vol. 17, pp.1177-1182.

20. A. Ziaai, 1981, "Back Stresses in Monotonic and Cyclic Deformation: Transient and Steady State Behavior," Ph.D. dissertation, Stanford University.

21. C.N. Ahlquist and W.D. Nix, 1971, "The Measurement of Internal Stresses During Creep of Al and Al-Mg Alloys," *Acta Met.*, Vol. 19, pp. 373-385.

22. M. McLean, 1980, "Friction Stress and Recovery During High Temperature Creep: Interpretation of Creep Transients Following a Stress Reduction," *Proc. R. Soc. London*, Series A, Vol. 371, 279-294.

DATE
FILMED
12/27/93
END